Inserting a Low-Refractive-Index Dielectric Rear Reflector into PERC Cells: Challenges and Opportunities

Preprint

Jonathan L. Bryan[1], Lejo Joseph Koduvelikulathu[2], Zih-Wei Peng[2], Joe V. Carpenter III[1], Michael G. Deceglie[3], Timothy J. Silverman[3], and Zachary C. Holman[1]

1 Arizona State University
2 International Solar Energy Research Center Konstanz e.V.
3 National Renewable Energy Laboratory

Inserting a Low-Refractive-Index Dielectric Rear Reflector into PERC Cells: Challenges and Opportunities

Preprint

Jonathan L. Bryan[1], Lejo Joseph Koduvelikulathu[2], Zih-Wei Peng[2], Joe V. Carpenter III[1], Michael G. Deceglie[3], Timothy J. Silverman[3], and Zachary C. Holman[1]

1 Arizona State University
2 International Solar Energy Research Center Konstanz e.V.
3 National Renewable Energy Laboratory

NOTICE

Inserting a Low-Refractive-Index Dielectric Rear Reflector into PERC Cells: Challenges and Opportunities

Jonathan L. Bryan[1], Lejo Joseph Koduvelikulathu[2], Zih-Wei Peng[2], Joe V. Carpenter III[1], Michael G. Deceglie[3], Timothy J. Silverman[3], Zachary C. Holman[1]

[1]School of Electrical, Computer, and Energy Engineering, Arizona State University, Tempe, AZ, 85287, USA

[2]International Solar Energy Research Center Konstanz e.V., 78467 Konstanz, Germany

[3]National Center for Photovoltaics, National Renewable Energy Laboratory, Golden, CO, 80401, USA

Abstract — One of the simplest and most effective ways to reduce the operating temperature of photovoltaic systems in the field is to reflect unusable, "sub-bandgap" light with energies below the cell absorber's bandgap energy. In this work, low-refractive index SiO_2 nanoparticle films inserted between c-Si wafers and metal electrodes significantly increase the reflectance of sub-bandgap light in fabricated test structures. These films are then integrated into the standard PERC fabrication sequence, revealing that the reflection benefits remains after some processing steps but are lost in certain conditions. The SiO_2 nanoparticle films are easily ablated during laser contact opening, but are undesirably etched during post-laser cleaning. After Al metallization, the fully fabricated devices show enhanced sub-bandgap reflection when annealed at moderate temperatures, but energy-dispersive x-ray spectroscopy shows that high-temperature firing causes unwanted Al penetration into the SiO_2 nanoparticle film, compromising reflection.

Index Terms — crystalline silicon, optics, PERC solar cell, photovoltaic cells, photovoltaic systems, thermal management, energy yield, module temperature

I. INTRODUCTION

Reducing the operating temperature of photovoltaic (PV) modules in the field is an effective way to increase a PV system's lifetime [1] and energy yield [2]. One of the most promising methods to reduce module operating temperature is by rejecting incident radiation that is unusable by the device for electrical energy conversion; specifically, an ideal sub-bandgap reflector at the rear side of a solar cell is predicted to have up to a 3.8 K reduction in annual irradiance-weighted temperature in crystalline silicon solar cells [2]. Analysis by Vaillon et al. similarly found sub-bandgap reflectance to be a thermal management strategy worth pursuing [3]. Most parasitic absorption of sub-bandgap light occurs in the rear metal electrode in crystalline silicon (c-Si) solar cells, and a proven method to reduce it is to insert a low refractive index dielectric film between the c-Si substrate and metal [4-6]. These reflecting films are most effective when their thickness is over 200 nm and their refractive index is as low as possible — conditions that minimize the field strength of evanescent waves at the metal surface, thereby avoiding plasmonic absorption [7].

One method to achieve a target refractive index of a dielectric film is by controlling its porosity, the volumetric ratio of void to constituent material. This approach has been demonstrated using aerosol impaction-driven assembly (AIDA), a deposition technique that first aerosolizes constituent material before depositing it onto the substrate with an impaction velocity that may be controlled to tune porosity [8,9]. AIDA-deposited silicon nanoparticle (NP) films were previously tested by Boccard et al. as rear reflectors in silicon heterojunction (SHJ) cells and optical test structures [10]. These silicon NP films enabled reflectance of over 90% of sub-bandgap wavelengths when inserted between a c-Si wafer and Ag reflector, and were shown to improve rear reflectance in SHJ cells while simultaneously not degrading the fill factor or open-circuit voltage.

This work investigates silicon dioxide (SiO_2) NP films for use as rear reflectors in c-Si solar cells. SiO_2 NP films offer considerable advantages over Si NP films: greater resilience when contacting Al at high temperatures and lower refractive index for equivalent film porosity. In Boccard's study, when the refractive index of the Si NP film was below 1.5, the measured reflectance at 1200 nm was well below the predicted simulation results (30% absolute less reflectance for film with refractive index of 1.1). The discrepancy was attributed to the roughness of the NP film surface, which incited plasmonic absorption in the adjacent Ag. Since the refractive index of dense SiO_2 is lower than that of Si, it is easier to attain minimum refractive indices, which lead to maximum reflectance in devices, without resorting to extreme porosities that compromise smooth interfaces. These films are incorporated into a standard PERC—as opposed to the less-common SHJ—fabrication sequence, testing compatibility with subsequent solar cell processing.

II. EXPERIMENTAL METHODS

Low-refractive-index SiO_2 NP films were tested in optical test structures and within a standard PERC processing sequence. The SiO_2 NP films were deposited using the AIDA process previously mentioned [8]. The SiO_2 NPs were synthesized upstream of the deposition nozzle in a dusty plasma using silicon- and oxygen-containing precursors. A pressure gradient between the upstream synthesis chamber and low-pressure deposition chamber accelerates the SiO_2 NPs

through the slit-shaped nozzle, where they impact and adhere to the substrate. In the downstream deposition chamber, the substrate is translated beneath the nozzle to control deposition area, porosity, film thickness, and achieve a good uniformity. The stoichiometry and average primary particle size of the SiO_2 films is controlled with precursor gas flow rates and chamber pressure of the plasma reactor. In this work, the SiO_2 films were stoichiometric with average particle size approximately 5 nm, confirmed with energy-dispersive X-ray spectroscopy (EDXS) and transmission electron microscopy, respectively. The film thickness, porosity, and surface roughness were measured with a JA Woollam M2000 spectroscopic ellipsometer. A Bruggeman effective-medium approximation was used with SiO_2 and void as the model inputs. This characterization was similarly performed, and its accuracy verified, in previous work on other materials This characterization was similarly performed, and its accuracy verified, in previous work on other materials [8,10].

Before implementing the NP films in devices, optical test structures were made to demonstrate the reflectance benefits and expected optical performance limit of the final cells. Monocrystalline silicon substrates were double-side textured using standard KOH etching and cleaned with Piranha, RCA-B, and BOE before subsequent depositions. The front side of all samples was coated with an 80-nm-thick SiN_x anti-reflection coating, deposited with plasma-enhanced chemical vapor deposition. Several material stacks were tested on the rear side: NPs/Al, NPs/Ag, ITO/Ag, and Ag or Al references with no NPs, with the Al, Ag, and ITO layers sputtered in all cases. The target SiO_2 NP film properties were a refractive index of 1.4 and thickness of 275 nm. Somewhat high refractive index was used (1.4 instead of 1.1-1.2, which is achievable with AIDA) to ensure minimal surface roughness. Planar c-Si witness samples analyzed with ellipsometry confirmed the consistency of film properties from run to run.

To test their compatibility in PERC processing, SiO_2 NPs were deposited on the rear-side of PERC-like precursors fabricated at ISC Konstanz, as seen in Figure 1. The precursors consisted of p-type c-Si wafers with a phosphorus-diffused front surface and a standard SiO_2/SiN_x passivation stack on the rear side. The same SiO_2 NP film properties used in the optical test structures were targeted here: refractive index of 1.4, thickness of 275 nm, and minimal roughness (2nm measured with ellipsometry). SiO_2 NP films were deposited on eight 6" PERC precursor samples and two 5" front-side-polished c-Si substrates for process compatibility tests. Specifically, the tested process steps were laser contact opening, post-laser wet chemistry cleaning, and Al metallization. A Rolfin StarFemto FX laser was used to ablate the SiO_2 NP film and passivation stack for the laser contact opening. After contact opening, a 60 second dip in 2% HF/HCl was performed for cleaning. Full-area Al metallization was then deposited on the back side using three different techniques: screen print and high-temperature firing in belt furnace (850 °C peak temperature), screen print and

low-temperature drying (200 °C for 20 minutes), and sputtering. The reflectance of the fully fabricated cells and optical test structures was measured using a PerkinElmer Lambda 950 spectrophotometer. Select samples were cleaved and their cross-sections imaged with scanning electron microscopy (SEM) and EDXS, performed with a ZEISS Auriga microscope.
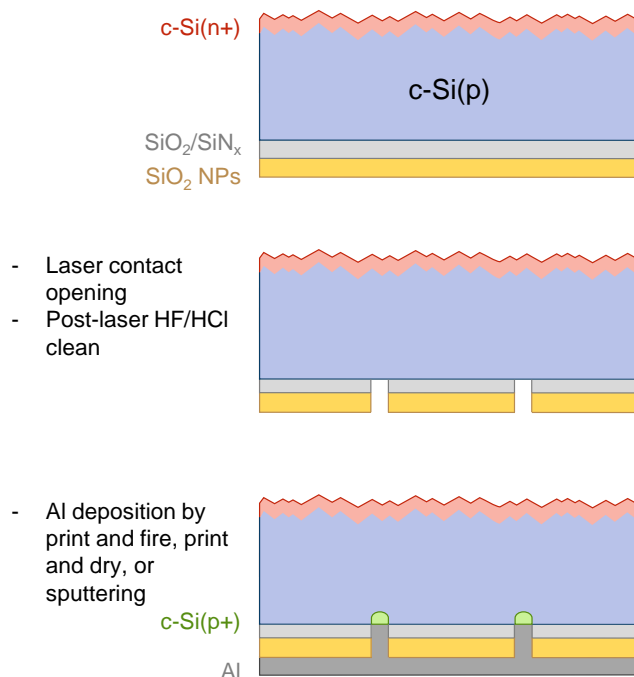

Fig. 1.   Schematic of the PERC cell fabrication steps.

III. RESULTS

A. Optical Test Structures

Figure 2 shows a schematic of the fabricated optical test structures and the reflectance of each sample. The results show that for both Al and Ag, reflectance values are significantly higher with the inclusion of the SiO_2 NP film, and both structures outperform the ITO/Ag reference. At 1200 nm, the reflectance of the Al-metallized test structures increased from 19.3 to 72.8% when the SiO_2 NP reflector is included. Since these test structures are double-side textured, and do not have heavily doped emitters or passivation stacks, this observed boost in reflectance is higher than expected when integrating the SiO_2 NP film in typical solar cell structures. Nonetheless, inclusion of these films within the optical test structures demonstrates promise to considerably reduce parasitic absorption in the rear metallized area in solar cells. Successful integration of these structures in solar cells is expected reduce operating temperature of PV modules in the field [2].
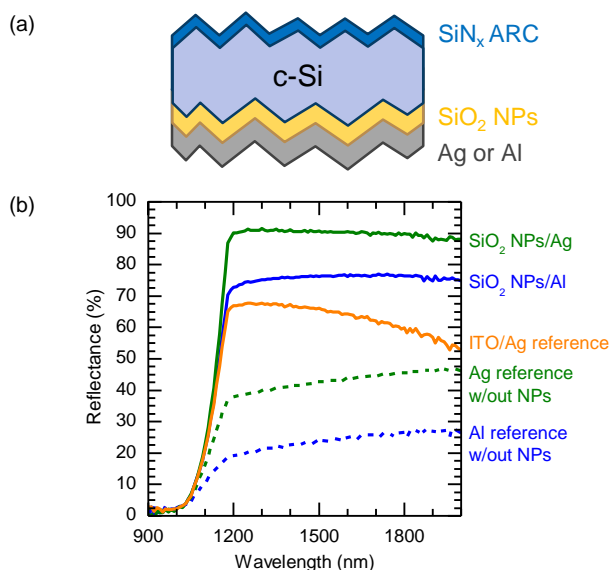
2

Fig. 2. (a) Schematic of the test structures used to measure reflectance and (b) the reflectance data of the test structures.

B. Laser Opening

Figure 3a shows the contact opening of the passivation stack without the SiO$_2$ NP reflector using ISC Konstanz's standard laser process with a fluence of 13.8 mJ/cm^2. As expected, a clean, fully opened point exposes the underlying c-Si wafer, which appears blue in the optical micrographs. This same laser recipe was used on the structure with a SiO$_2$ NP film, shown in Figure 3b. It is evident that this laser process had insufficient
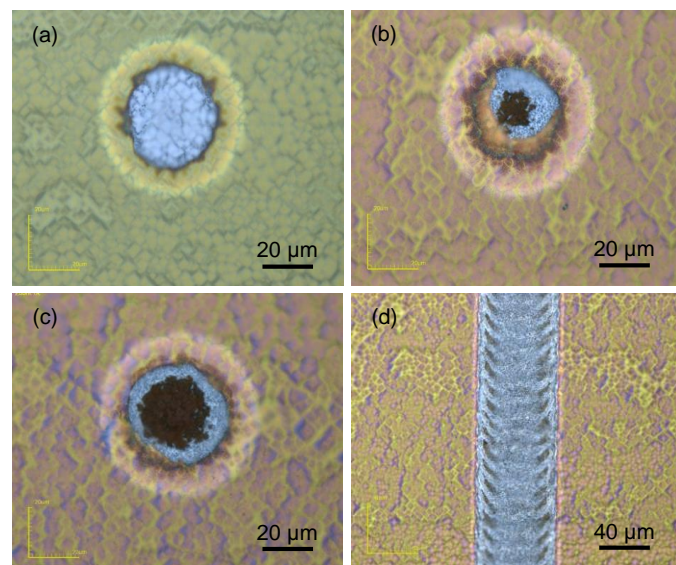

Fig. 3. Optical microscope images after laser ablation for (a) standard PERC passivation stack without SiO$_2$ NP film at baseline laser fluence, (b) PERC passivation stack with SiO$_2$ NP film at baseline laser fluence, (c) PERC passivation stack with SiO$_2$ NP film at higher laser fluence, and (d) PERC passivation stack with SiO$_2$ NP film at higher laser fluence and with linear translation showing good contact opening.

power to create an opening to the c-Si substrate. Instead, it appears the SiO$_2$ NP film absorbed the laser energy and melted, forming the dark brown region in the center of the ablated area, which would impede contact formation. Increasing the laser fluence from 13.8 to 18.5 mJ/cm^2 appears to exacerbate this issue for the point ablation, as seen in Figure 3c. However, for linear contact openings, the translated laser can evaporate the SiO$_2$ residue, resolving the problem; Figure 3d shows a clear linear opening to the c-Si wafer with the increased laser power (18.5 mJ/cm^2).

C. Post-Laser Cleaning

The planar samples with SiO$_2$ NP films were dipped for various times in an HF/HCl cleaning solution designed to remove passivation film residue formed in the laser process he planar samples containing SiO$_2$ NP films were dipped in the HF/HCl laser cleaning solution for various times. After each dip, the SiO$_2$ NP films were measured with ellipsometry. Figure 4 shows the average film thickness after the cleaning times and reveals that the NP films were rapidly etched in the cleaning solution. This is substantiated by photos of the samples, which underwent drastic color changes as the interference condition shifted with the optical thickness of the film, as also seen in Figure 4. This result represents a challenge, as significant reduction in SiO$_2$ NP film thickness will reduce its efficacy as a rear reflector. Further studies investigating the etch rate of films composed of NPs of other (low-refractive-index) materials, such as MgF$_2$, could reveal pathways to mitigate or eliminate film loss. Since the etch rate was extremely fast, the post-laser cleaning step was skipped for samples before Al metallization.
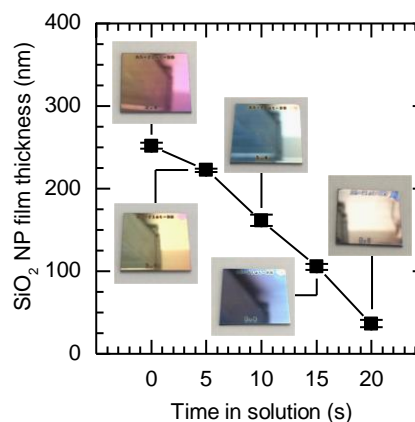

Fig. 4. SiO$_2$ NP film thickness after dipping in HF/HCl post-laser cleaning solution.

D. Al Metallization

As previously described, three Al metallization methods were tested to compare their performance. Figure 5 shows the reflectance of the PERC precursor samples after each metallization sequence, with and without the SiO$_2$ NP film.
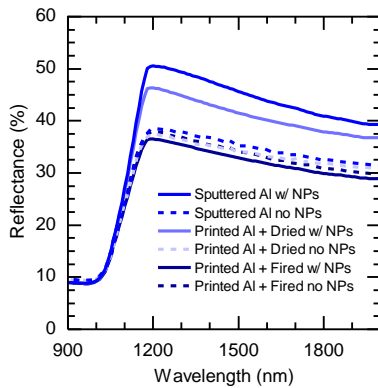
3

Fig. 5. Reflectance data of the fully fabricated PERC structures with and without SiO$_2$ NPs.

The data reveals that sputtered Al exhibits a greater reflectance boost compared to both screen-printed Al structures. The reflectance at 1200 nm for the sputtered, dried, and fired samples with SiO$_2$ NPs is 50.5, 46.4, and 36.5%, respectively. The reason the sputtered Al sample does not reach the 72.8% reflectance seen in the test structure is that the PERC precursor, with its planar rear side and heavily doped layers, has infrared parasitic absorption occurring in regions besides the rear reflector. The optical role of the SiO$_2$/SiN$_x$ passivation stack can be seen in the sputtered Al sample without NPs; at 1200 nm, the reflectance in the cell was 1200 nm, while the Al test structure reference was 19.3%. This optical difference between PERC and Al-BSF, a consequence of the properties of the passivation stack, was found to appreciably reduce operating temperature in simulation and indoor testing [11]. The most striking aspect of the reflectance data is the observed reduction in reflectance for the cell that underwent high-temperature firing after Al screen-printing.

Figure 6, which is an SEM image and compositional map from the fired sample, shows clear evidence that Al from the paste micro-particles has penetrated into the SiO$_2$ NP film. This Al diffusion likely affects the optical properties of the
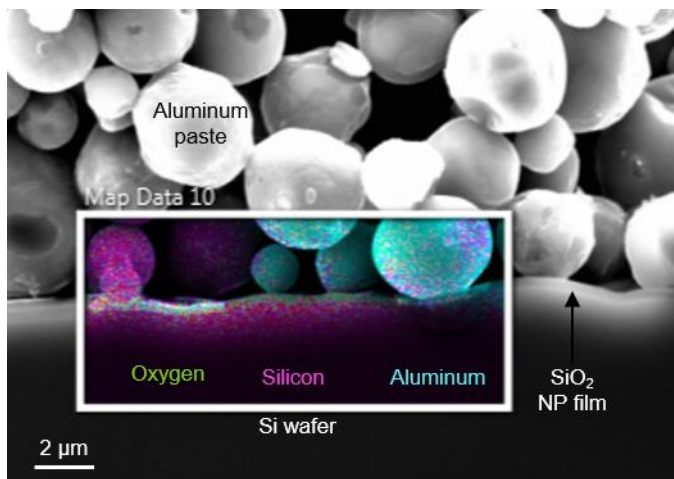

Fig. 6. SEM image with EDXS of PERC structure with SiO$_2$ NP film after Al screen printing and high-temperature firing.

reflector layer, explaining the observed decrease in reflectance. Since the (low-temperature) dried samples did not suffer from this reflectance degradation, further studies of processing compatibilities at intermediate firing temperature ranges should be performed.

IV. CONCLUSIONS

SiO$_2$ NP films, when incorporated on the rear side of c-Si PV cells, significantly increase sub-bandgap reflectance. This study represents the initial findings for adopting such films into PERC processing technology to enhance thermal management in fielded modules. While some processes showed no or benign effects from the addition of the NP film, the post-laser etching and high-temperature firing steps were particularly detrimental to its stability. A logical next step is further studies on the relationship between film properties, such as stoichiometry and pore size, and chemical stability during these processes. Since the reflectors can considerably reduce parasitic absorption and thus module operating temperature, overcoming these remaining processing challenges can lead to higher PV system energy yield.

REFERENCES

[1] S. Kurtz, K. Whitfield, G. TamizhMani, M. Koehl, D. Miller, J. Joyce, J. Wohlgemuth, N. Bosco, M. Kempe, and T. Zgonena, "Evaluation of high-temperature exposure of photovoltaic modules," *Prog. Photovolt., Res. Appl.,* vol. 19, no. 8, pp. 954-965, 2011.

[2] T. J. Silverman, M. G. Deceglie, I. Subedi, N. J. Podraza, I. M. Slauch, V. E. Ferry, and I. Repins, "Reducing Operating

4

Temperature in Photovoltaic Modules," *IEEE J. of Photovoltaics* 8, 532, 2018.

[3]   R. Vaillon*, O. Dupré, R. B. Cal, and M. Calaf, "Pathways for mitigating thermal losses in solar photovoltaics," *Sci. Rep.,* vol. 8, no. 1, Art. no. 13163, 2018.

[4]   Z. C. Holman, M. Filipič, A. Descoeudres, S. De Wolf, F. Smole, M. Topič, and C. Ballif, "Infrared light management in high-efficiency silicon heterojunction and rear-passivated solar cells," *J. Appl. Phys.,* vol. 113, p. 013107, 2013.

[5]   Z. C. Holman, A. Descoeudres, S. De Wolf, and C. Ballif, "Record Infrared Internal Quantum Efficiency in Silicon Heterojunction Solar Cells with Dielectric/Metal Rear Reflectors," *IEEE J. Photovoltaics*, vol. 3, pp. 1243-1249, 2013.

[6]   Z. C. Holman, M. Filipič, B. Lipovšek, S. De Wolf, F. Smole, M. Topič, and C. Ballif, "Parasitic absorption in the rear reflectors of silicon solar cells: Simulation and measurement of the sub-bandgap reflectance for common dielectric/metal reflectors," *Solar Energy Mater. Solar Cells,* vol. 120, pp. 426-430, 2014.

[7]   Z. C. Holman, S. De Wolf, and C. Ballif*.,* "Improving metal reflectors by suppressing surface plasmon polaritons: A priori calculation of the internal reflectance of a solar cell," *Light: Sci. Appl.* vol 2, p. e106, 2013.

[8]   P. Firth and Z. C. Holman, "Aerosol Impaction-Driven Assembly System for the Production of Uniform Nanoparticle Thin Films with Independently Tunable Thickness and Porosity", ACS Appl. Nano Mater., vol. 1, no. 8, pp. 4351-4357, 2018.

[9]   Z. C. Holman and U. Kortshagen, "A flexible method for depositing dense nanocrystal thin films: Impaction of germanium nanocrystals," *Nanotechnology,* vol. 21, p. 335302, 2010.

[10] M. Boccard, P. Firth, Z. J. Yu, K. C. Fisher, M. Lailaeioun, S. Manzoor, and Z.C. Holman, "Low-refractive index nanoparticle interlayers to reduce parasitic absorption in metallic rear reflectors of solar cells," *Physica Status Solidi*, vol. 214, issue 10, 2017.

[11] M. R. Vogt, H. Schulte-Huzel, M. Offer, S. Blankemeyer, R. Witteck, M. Köntges, K. Bothe, and R. Brendel "Reduced module operating temperature and increased yield of modules with PERC instead of Al-BSF solar cells," *IEEE J. Photovolt.*, vol. 7, no. 1, pp. 44-50, Jan. 2017.